Materials Advances

ROYAL SOCIETY OF CHEMISTRY

PAPER

View Article Online
View Journal | View Issue

Cite this: *Mater. Adv.*, 2024, 5, 6132

Effect of density and thickness of flexible polyurethane foam on the performance of triboelectric nanogenerators†

Ahmed Abdelhamid Maamoun,[a] Ahmed Adel Mahmoud,[a] David Magdy Naeim,[b] Mustafa Arafa *[b] and Amal M. K. Esawi [b]

Triboelectric nanogenerators (TENGs) offer an attractive approach for energy harvesting for self-powered devices. Improving the output performance of TENGs depends on many factors, including the density and thickness of the materials used. In this study, flexible polyurethane foam (FPU) with different densities of 17, 22, 26, and 33 kg m^{-3} was fabricated by altering the isocyanate index and water content during preparation and the effect on the TENG's output voltage was investigated. Additionally, the effect of changing the thickness of FPU (namely, 4, 6, 8, and 10 mm) for each density on the TENG's output voltage was also examined. The chemical structure and pore morphology of the FPU foams were investigated using FTIR and FESEM. The findings of the study indicate that increasing the isocyanate index and water content led to the formation of larger cavities and pores, resulting in reduced densities and increased porosity. In addition, the compression test results demonstrated that the compressive strength of FPU foam increased as the isocyanate index and water content decreased. The results obtained from the TENG device showed that increasing the applied frequency and the FPU density caused an increase in the output voltage, while increasing the thickness resulted in a drop in the output voltage. Therefore, FPUs with a higher density (33 kg m^{-3}) and a smaller thickness (4 mm) produce a higher output voltage. In addition, the FPU-based TENG achieved a maximum power density of 0.025 mW cm^{-2} under the conditions of a 5 Hz frequency, 20 MΩ resistance, and 4.8 N force. The TENG device effectively charged a 10 μF capacitor to 15.4 V in approximately 60 seconds, storing 1185.8 μJ of energy. This energy was utilized to illuminate four white commercial LEDs connected in series. Hence, the FPU-based TENG has promising prospects for applications involving the powering of electronics and energy storage.

Received 22nd March 2024,
Accepted 18th June 2024

DOI: 10.1039/d4ma00304g

rsc.li/materials-advances

1. Introduction

Exploiting renewable energy has gained increased relevance in light of the continuous development of the global economy, the depletion of non-renewable resources, and the threat of environmental deterioration.[1,2] As a result, considerable efforts have been made to find alternative and sustainable sources of energy in order to mitigate these challenges.

Triboelectric nanogenerators (TENGs) are a category of sustainable energy harvesting devices that function by leveraging the triboelectric effect, a phenomenon characterised by the exchange of electrons between two materials with distinct electronegativities.[3] TENGs can enable electrical energy generation without the requirement of an external power source, making them a viable and promising approach for the production of sustainable energy.[4] They can be constructed using various techniques, including freestanding, single electrode, lateral sliding, and vertical contact separation.[5] Due to its high efficiency, ease of use, and high stability, vertical contact separation is the most popular of these techniques and is therefore a good choice for a variety of applications in energy harvesting and self-powered sensing.[6–8] Several factors, including materials used, contact area, contact force, and separation distance, can be adjusted to control and optimize the output of TENG devices.[9]

The operating principle of TENGs relies on electrostatic induction and triboelectrification between two tribopolar materials with distinct triboelectric properties: one with a tendency to donate electrons (referred to as tribopositive), and the other

[a] Department of Engineering Physics and Mathematics, Chemistry Division, Faculty of Engineering, Ain Shams University, 1 EL-Sarayat Street-Abdo Basha Sq., Cairo, 11517, Egypt
[b] Department of Mechanical Engineering, The American University in Cairo, AUC Avenue, P.O. Box 74, New Cairo 11835, Egypt. E-mail: mharafa@aucegypt.edu

† Electronic supplementary information (ESI) available. See DOI: https://doi.org/10.1039/d4ma00304g

tends to accept electrons (referred to as tribonegative). When these materials come into contact, electrons are transferred from one material to the other, resulting in charge separation. Due to the charge imbalance, the separation of the materials generates an electric field that can derive electrons through an external circuit and produce an electrical current.[10,11] Metals have traditionally been utilized as tribopositive materials in TENGs because of their high conductivity. However, the use of metals in TENGs is associated with several disadvantages, such as corrosion, degradation, and oxidation.[12,13] These factors can result in a decline in the performance of TENGs over time. Therefore, it is essential to seek alternative materials that offer both durability and high electrical output for TENG applications. Generally, porous polymeric materials are more efficient in TENG than dense and compact materials because charges are induced not only on the material's surface, but also from the material's inner pores during deformation, resulting in a higher electrical output.[14] In 2014, foams were first incorporated into TENGs to harness the benefits of their porous nature.[15] Lee *et al.*[16] demonstrated the successful fabrication of a hydrophobic sponge based TENG, utilizing a polymer composite of polydimethylsiloxane (PDMS) and polystyrene foam. Their findings revealed that the TENG device produced an output of 130 V and 100 μA cm^{-2} at 90 N. Kamaruzaman *et al.*[17] investigated the utilization of recycled polystyrene (rPS) foam combined with zinc oxide (ZnO) nanoparticles for applications in TENG devices. Their findings revealed that the untreated rPS generated an output voltage of 3.8 V at 2 N with a power density of 6.2 μW cm^{-2}. In contrast, the rPS-ZnO composite TENG demonstrated significant performance improvements, achieving an output voltage of 8.2 V (a two-fold increase) and a power density of 28.1 μW cm^{-2} (a 4.5-fold enhancement). Ren *et al.*[18] developed a TENG using foam and polyvinyl chloride (PVC) as triboelectric materials. Their findings demonstrated that the device achieved an open-circuit voltage of 224.26 V and a short-circuit current of 2.74 mA. Wu *et al.*[19] designed a sensor-based TENG by combining porous PDMS foam and serpentine silver nanowires. This device yielded an open circuit voltage of 78.7 V when subjected to a contact force of 10 N.

Among all foam materials, flexible polyurethane (FPU) is a promising material characterized by its unique three-dimensional porous network that can be used in TENG devices for various applications. FPU exhibits several desirable characteristics, such as versatility, functionality, porosity, lightweight, breathability, flexibility, compressibility, durability and low cost compared to other porous materials.[20] FPU is a synthetic polymer composed of urethane (NHCOO) moieties.[21] It has various applications, including sound absorption,[22] bedding,[23] and automotive interior.[24] The architecture of FPU foam consists of soft and hard segments, which provide flexibility and rigidity, respectively.[25] The synthesis of FPU involves two significant reactions: one is between polyol (OH) and diisocyanate (NCO) to yield NHCOO, named gelling reaction, and the other is between NCO and water to produce carbon dioxide (CO_2), urea and biuret linkages, termed the blowing reaction.[26,27] The two reactions occur simultaneously, and their rate depends on temperature, amount of blowing agent and isocyanate index. The isocyanate index, represented by the (NCO/OH) ratio, influences the density and mechanical performance of the FPU foam.[28] An increase in the isocyanate index and in water content, leads to an increase in the blowing reaction and consequently a reduction in the foam density. Furthermore, it has been shown that an increased isocyanate index is associated with a greater rigidity in the FPU foam, whereas a decreased isocyanate index leads to a higher level of elasticity. Hence, changing the isocyanate index during the preparation of FPU foam can provide a degree of control over its properties, which can be advantageous for its use as a tribopositive layer in TENGs.

Several investigations have been conducted to enhance the electrical characteristics of FPU foam by the use of fillers during the synthesis process or by the application of surface coatings. Weldemhret *et al.*[20] for instance, demonstrated that incorporating carbon into FPU foam could improve its electrical properties. The findings of their study revealed that FPU/carbon composites generated an output of 36 V and 100 V while walking and running, respectively, at a contact force of 20N and a frequency of 6 Hz. These results indicate the promising potential of such composites in shoe insoles. The current authors modified FPU foam through the incorporation of natural montmorillonite (Na-MMT) nanoclay at different weight ratios (0.1, 0.3, 0.5, and 0.7 wt%) and reported an output voltage of 164 V for the FPU/Na-MMT0.3 when tested at a force of 4.8 N and a frequency of 5 Hz corresponding to an increase of 62.37% compared to pristine FPU.[29] Liu *et al.*[30] studied the effect of polyaniline coating on the electrical properties of FPU foam. They reported that the modified material could produce an output of 570 V at 60% deformation, due to the polyaniline coating's high contact area. Nevertheless, it is important to note that both methods have their own limitations, since the presence of excessive filler material might potentially lead to agglomeration, hence negatively impacting the cellular structure of the foam.[29,31] On the other hand, surface coatings have a physical bond with the polymer matrix and are susceptible to degradation when exposed to water.[20] In addition, the application of coatings involves a significant investment of time and capital. The aforementioned drawbacks can have a detrimental effect on the long-term effectiveness of TENG. Consequently, it is crucial to develop strategies that enhance the flexibility and durability of FPU foam without compromising its mechanical properties. One approach involves modifying the isocyanate index and water content during the production process of FPU which is expected to significantly impact the characteristics of the foam, including density, functionality, porosity, and mechanical performance. This, in turn, can influence the FPU foam's electrical characteristics.

The objective of the current study is to investigate the impact of modifying the isocyanate index and water content during FPU foam fabrication on the performance of TENG. The purpose is to determine the optimal formulation that yields the maximum output voltage when implemented in the TENG

device. In addition, an investigation was conducted to assess the impact of different FPU thicknesses on the generated output voltage of the TENG. Moreover, the prepared material's chemical structure, morphology, porosity, density, thermal stability, and compression performance were also studied. Finally, the fabricated FPU-based TENG device was characterized by measuring the output voltage, current, and power density under varying load resistances.

2. Experimental section

2.1 Materials

Different densities from FPU foam were fabricated using polyether polyol, marketed under the trade name of Desmophen 1905 N, provided by Covestro Co. (Germany) with an OH number of 41.5–45.5 mg of KOH per g, styrene-acrylonitrile solid content 10 wt%. Lupranate T80, a mixture of 80% 2,4 and 20% 2,6 toluene diisocyanate (TDI) with an NCO content of 48.2 wt % and a molecular weight of 174.2 g mol^{-1}, was used as the diisocyanate and was supplied by BASF polyurethanes (Germany). Struksilon 8146 was used as stabilizer, supplied by Schill + Seilacher GmbH (Germany). Struksilon Amine 33, a compound of 33.3% triethylenediamine and 66.7% dipropylene glycol, was employed as amine catalyst, purchased from Schill + Seilacher GmbH (Germany). Stannous octoate was provided by Air product (UK) as Dabco T-9. The chemical blowing agent used was distilled water sourced from our laboratory.

2.2 Synthesis of FPU foam with different densities

FPU foams of varying densities were synthesized using a laboratory-scale one-shot process. The polyol was dried for 24 hours at 105 °C to eliminate any residual moisture and subsequently cooled to ambient temperature. The polyol was combined with a distilled water-blowing agent in several weight ratios, specifically 4.75, 5.5, 6.2, and 6.5 wt %. Additionally, silicon surfactant, tertiary amine and stannous octoate were added in different ratios for each formulation, as specified in Table 1. The ratios were adjusted in order to regulate the exothermic reaction and the amount of rise in foam level. The mixing process was conducted in a polypropylene vessel for 50 seconds at a rotational speed of 1000 rpm. To ensure the thorough dispersion of the catalysts, the amine and stannous octoate were diluted in the polyol, utilizing ratios of 1 : 3 and 1 : 2 by weight, respectively, prior to their incorporation. Subsequently, TDI was introduced into the polyol system and vigorously stirred for 7 seconds at 3000 rpm. Fig. 1a presents a schematic of the process employed for the production of FPU foam. The resulting mixture was promptly poured into a mould measuring 200 × 200 × 150 mm, and the foam was allowed to rise freely and cure for 48 hours prior to being sectioned for measurements. The reaction scheme of FPU preparation is illustrated in Fig. 1b. The amount of TDI was calculated according to the following equation:

$$m_{(\mathrm{TDI})} = \left[\frac{I_{(\mathrm{NCO})}}{100}\right]\left(\mathrm{Eq}_{(\mathrm{TDI})}\right)\left[\frac{m_{(\mathrm{polyol})}}{\mathrm{Eq}_{(\mathrm{polyol})}} + \frac{m_{(\mathrm{water})}}{\mathrm{Eq}_{(\mathrm{water})}}\right] \quad (1)$$

where $m_{(\mathrm{TDI})}$, m_{polyol}, represent the masses of isocyanate and polyol. $m_{(\mathrm{water})}$ refers to the mass of distilled water employed in the reaction. Furthermore, $\mathrm{Eq}_{(\mathrm{TDI})}$, $\mathrm{Eq}_{(\mathrm{polyol})}$ and $\mathrm{Eq}_{(\mathrm{water})}$ refer to the equivalent masses of isocyanate, polyol, and water, respectively. Meanwhile, $I_{(\mathrm{NCO})}$ represents the isocyanate index, which was varied to four different values: 1.05, 1.10, 1.15, and 1.20, resulting in the production of four distinct formulations denoted as FPU1.05, FPU1.10, FUP1.15 and FPU1.20.

Table 1 Formulations for preparing FPU foams

	Formulations (Pphp[a])			
Materials	FPU1.05	FPU1.10	FPU1.15	FPU1.20
Polyol	100	100	100	100
TDI	55	66	77	84
Distilled water	4.75	5.50	6.20	6.50
Silicon surfactant	1.95	2.20	2.23	2.40
Stannous octoate	0.5	0.48	0.56	0.65
Tertiary amine	0.95	0.64	0.75	0.63
Isocyanate index	1.05	1.10	1.15	1.20

[a] Pphp: part per hundred parts of polyol by weight.

2.3 Fabrication of FPU-based TENG

Fig. 1c illustrates the vertical contact separation mode exhibited by the TENG device. The construction of the TENG entailed the use of FPU foam, which served as a static layer, functioning as the tribopositive layer due to its electron-donating capability. Fig. 1d and e display the original shape of the prepared FPU and its degree of flexibility, respectively. In contrast, polytetrafluoroethylene (PTFE) film, a movable layer, was chosen as a tribonegative layer due to its superior electron-attracting capability. Aluminium (Al) adhesive tapes were employed to construct the electrodes on the upper and lower surfaces. Subsequently, the fabricated TENG device was connected to a digital oscilloscope in order to measure the output voltage. The contact area of the TENG device was 8 × 5.5 cm^2.

2.4 Characterization of the prepared FPU foams

The Thermo Scientific Nicolet FTIR instrument was utilized, employing attenuated total reflection (ATR) mode to examine the chemical structure of the prepared FPU foams. In transmission mode, four samples were scanned within the frequency range of 400–4000 cm^{-1}, with a resolution of 4 cm^{-1}. A field-emission scanning electron microscope (FESEM, Thermo Scientific Quattro S) was employed to investigate the morphology of the produced FPU foams. The analysis was conducted under a magnification of 50× and an accelerating voltage of 10 kV. ImageJ software was used to analyze the SEM images and obtain the average pore and cavity diameters. The porosity of the FPU foams was evaluated using the following formula:

$$\mathrm{Porosity} = \frac{V_{\mathrm{w}}}{V_{\mathrm{t}}} \quad (2)$$

where V_{w} and V_t represent the volume of water contained within the sample and the sample's total volume, respectively.

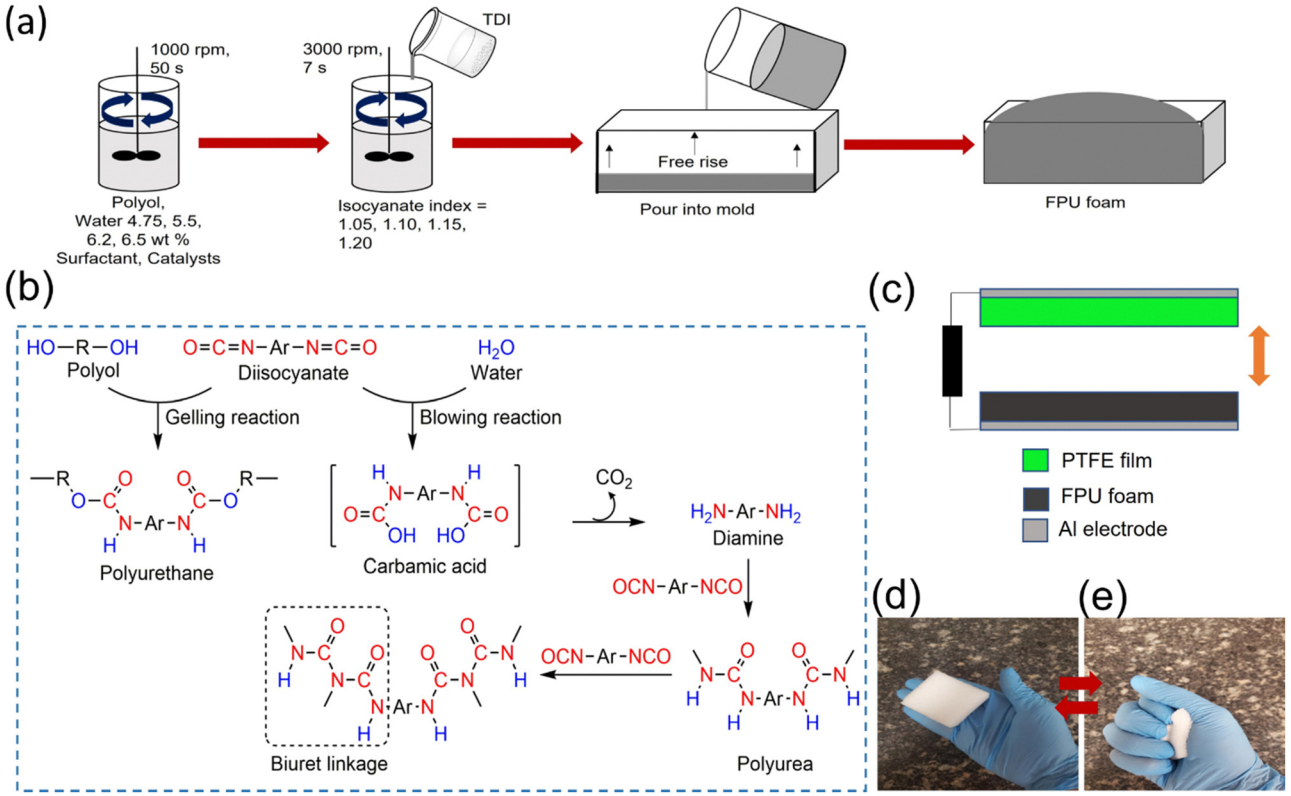

Fig. 1 Schematic representation of (a) the synthesis protocol of FPU foam with different isocyanate index and water content, (b) the preparation scheme of FPU foam, (c) the construction of TENG, (d) the original shape of FPU sample, and (e) the compressed FPU sample by hand, demonstrating its flexibility and elasticity.

The apparent density of FPU foams was calculated as the mass-to-volume ratio of a sample taken from the midsection of the foam block. The thermal decomposition behavior of FPU foam was studied using a LABSYS EVO TGA (SETARAM) instrument. Differential thermogravimetric analysis (DTG) data were also reported. Samples were deposited in platinum pans and heated in nitrogen gas at a constant rate of 10 °C min^{-1} between 25–600 °C. The compression strength of FPU foams was assessed using the ZwickRoell/Z100 universal testing machine, in accordance with the testing procedure specified in the ASTM D-3574-17 test C. The cell load applied was 1 kN, with a crosshead displacement rate of 50 mm min^{-1} and a deformation level of 50%. The sample dimensions were 50 × 50 × 40 mm^3 (length × width × height). The effect of modifying the density and thickness of the FPU foams on the output voltage of the TENG was investigated.

Mechanical testing was conducted by mounting the FPU foam sample on a rigid horizontal surface while attaching an upper PTFE film to a cam-operated oscillating arm that causes cyclic contact and separation between the layers. The cam is driven by an electric motor whose speed is varied to test the device at different frequencies. In addition, the applied force was measured by a straight bar load cell. The output voltage was measured using a mixed domain oscilloscope (Tektronix MDO 3024).

The magnitude of the voltage signal was evaluated over a complete cycle, from peak to peak, at three distinct forces of 3.8 N, 4 N, and 4.8 N and frequencies of 2.5 Hz, 3.75 Hz, and 5 Hz. Four densities of FPU were prepared and examined, and the influence of four different thicknesses (4, 6, 8, and 10 mm) from each density on the output voltage of the TENG device was studied.

3. Results and discussion

3.1 Fourier transform infrared (FTIR) spectroscopy

FTIR spectroscopy was used to investigate the chemical structure of the produced FPU foam. Fig. 2a–d illustrates the typical FTIR pattern for FPU foam samples. The FTIR spectra exhibit all the well-defined bands that are characteristic of FPU foam: the band at 3280 cm^{-1} is attributed to urethane (–NH) stretching vibrations,[32] whereas the bands at 2970 and 2807 cm^{-1} are attributed to asymmetric and symmetric aliphatic (C–H) stretching vibrations of CH_2 groups, respectively.[33] All samples exhibited a band at 2275 cm^{-1} ascribed to unreacted NCO groups.[34] In addition, the band at 1720 cm^{-1} is attributed to unbonded urethane carbonyl groups (C═O) stretching vibrations, the band at 1640 cm^{-1} to monodentate H-bond urea C═O groups,[35] the band at 1533 cm^{-1} to N–H bending vibrations, the band at 1296 cm^{-1} to C–H bending vibrations of $–CH_3$ groups, and the band at 1089 cm^{-1} to C–O–C stretching vibrations.[22,36]

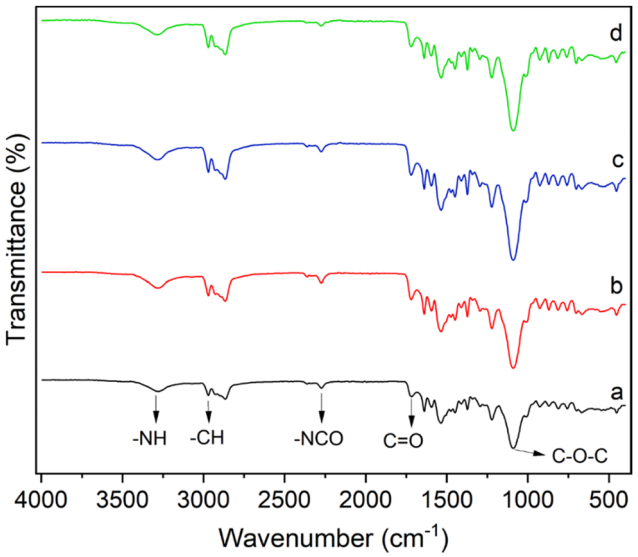

Fig. 2 Typical FTIR spectrum of (a) FPU1.05 (b) FPU1.10 (c) FPU1.15 and (d) FPU1.20.

3.2 Scanning electron microscopy (SEM) analysis

The effect of changing the isocyanate index and water content on the morphological structure of FPU foam was investigated. The SEM micrographs of the FPU foams are presented in Fig. 3. It is worth noting that all samples display cavities and pores of varying sizes. The mechanism of cavity formation can be explained as follows: the reaction between isocyanate and water initiates the generation of CO_2 gas, which subsequently expands until it encounters adjacent cavities. Pores are formed when the narrow hollow walls cannot withstand pressure from either side. The type of pores that emerge is contingent upon the cavity walls' thickness and the liquid and gas drainage flow rate. Closed pores develop when the polymerization reaction is completed prior to the rupture of the cavity walls; in this case, the walls of cavities are strong enough to withstand the gas pressure. Conversely, open pores arise due to the reduced strength of the walls and a high flow rate of drainage within the thin cavity walls. On the other hand, partial open pores occur when the wall strength is elevated, and the drain flow rate is low; in this case, the pores may be neither fully closed nor completely open.[37–39]

It was found that increasing isocyanate index and water contents resulted in the formation of larger cavities and pores, as presented in Table 2. The average cavity diameter for FPU1.05 was 0.562 ± 0.058 mm. Increasing the isocyanate index and water content increased cavity diameter by 24.02%, 28.29%, and 56.93% for FPU1.10, FPU1.15, and FPU1.20, respectively. The average pore diameter followed the same trend. This is because decreasing the isocyanate index and the water content in FPU foam formulations limits the generation of CO_2 gas during the foam rise. This, in turn, decreases the growth of foam cavities, producing foam with smaller cavities and pores. Therefore, it is crucial to carefully adjust the ratios to achieve the desired cellular structure that gives the highest output voltage.

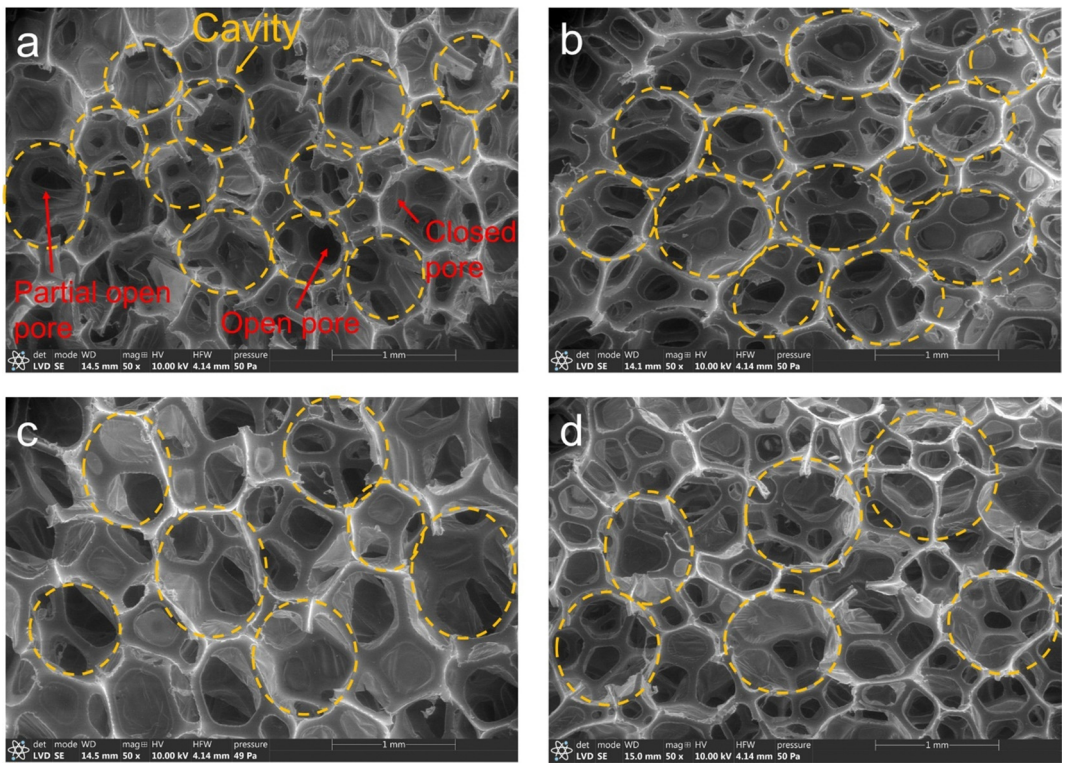

Fig. 3 SEM micrographs of (a) FPU1.05, (b) FPU1.10, (c) FPU1.15 and (d) FPU1.20.

Table 2 Average cavity and pore diameters of different densities of FPU foam

Sample	Average cavity diameter (mm)	Average pore diameter (mm)
FPU1.05	0.562 ± 0.058	0.197 ± 0.075
FPU1.10	0.697 ± 0.084	0.25 ± 0.1
FPU1.15	0.721 ± 0.103	0.271 ± 0.08
FPU1.20	0.882 ± 0.047	0.275 ± 0.09

3.3 Porosity

The porosity of FPU foam is a significant attribute that is expected to have a direct impact on the performance output of TENGs. Typically, porous materials have superior output performance in comparison to compact materials[13,15,40,41] due to the improved contact area and electrostatic induction between the triboelectric layers during the process of cyclic contact separation. Table 3 presents the values for the open porosity of the prepared FPU foams. It is clearly observed that the porosity increases with the increase in isocyanate index and water ratios. This can be attributed to enhanced CO_2 gas generation from the isocyanate-water reaction, which produces more pores during foam rise resulting in a cellular structure that is less dense. However, it is essential to carefully optimize the isocyanate index and water ratios during FPU production in order to prevent the formation of excessive voids/pores and attain the necessary balance between porosity and other material properties, particularly for use in TENG devices.

3.4 Apparent density

The output voltage of the TENG device is expected to be significantly influenced by the FPU foam's density. This is because the density significantly impacts the contact surface area between triboelectric layers during the periodic contact separation process. The measured densities of the prepared FPU foams were calculated and presented in Table 3. It was found that increasing the isocyanate index and water content reduces the density of FPU foam. This can be attributed to the shift of the reaction towards increased blowing and less gelling. Consequently, a greater amount of carbon dioxide gas is produced. As a result, cell volume experiences an increase, leading to a reduction in density.

3.5 Thermogravimetric analysis (TGA)

Prior to fabricating the TENG device, it is crucial to measure the thermal stability of the FPU foams to ensure that the developed foams can resist temperature fluctuations without deterioration. While temperature variations during TENG operation are not our focus in the present study, these may result from environmental conditions or periodic contact between two triboelectric layers, potentially affecting their stability and overall performance. The thermal stability of the manufactured FPU foams was examined using a TGA instrument in a nitrogen gas atmosphere. Fig. 4 demonstrates the TGA/DTG plots for the FPU samples. In addition, the thermal decomposition data, such as the temperature at which 5% and 50% of the mass is lost ($T_{5\%}$ and $T_{50\%}$, respectively), and the maximum decomposition temperatures (T_{max1} and T_{max2}) were determined and presented in Table 4. It is clearly noticed that the thermal degradation profiles for FPU samples revealed two primary decomposition stages with two maximum temperatures that are characteristic of FPU foams. The first stage, which falls within the temperature range of 250–350 °C, corresponds to the decomposition of hard domains such as urethane and urea.[25] The urethane moieties are known to be thermally unstable, and the polyurethane structure influences its decomposition temperature.[42] The urethane segment degrades *via* three scenarios: dissociation into isocyanate and polyol precursors, formation of carbamic acid and olefin with subsequent dissociation of carbamic acid into primary amine and carbon dioxide, and a formation of a secondary amine and carbon dioxide.[43] On the other hand, the second stage, which occurs between 350–450 °C, is associated with the degradation of the polyol's soft segments.[44]

It was found that increasing isocyanate index, specifically in the range of 1.05–1.15, and water content significantly improved the FPU foam's thermal stability. The evidence for this enhancement is provided by a gradual increase in $T_{5\%}$, $T_{50\%}$, and T_{max1} values for FPU1.05, FPU1.10, and FPU1.15, as shown in Table 4. The enhanced thermal stability is ascribed to the development of an ordered pi-stacking network structure, which is a result of the aromatic rings present in TDI. This is facilitated by the higher NCO/OH ratio. This structural arrangement imparts some degree of rigidity, and stiffness, to the foam, delaying the onset of thermal deterioration and consequently increasing the thermal stability. However, FPU1.20 displayed a decrease in the thermal stability compared to other foam samples, possibly due to excess NCO by 20% promoting the formation of more volatile products, which accelerate degradation and hence decrease the thermal stability, as shown in Table 4. Finally, T_{max2} revealed no significant change since it mainly relies on the nature of the polyol employed, which remains the same across all formulations (see Table 1).

Table 3 Open porosity and density values of the obtained FPU foams

Sample	Porosity (%)	Density (kg m^{-3})
FPU1.05	69.6 ± 0.99	33
FPU1.10	74.5 ± 1.04	26
FPU1.15	77.1 ± 0.86	22
FPU1.20	82.7 ± 0.49	17

3.6 Compression behavior

Fig. 5 presents the compression stress–strain curves of the prepared FPU foam at 50% deformation level. The compression plots showed three distinct regions: The first is elastic deformation (0–10%), wherein the stress and strain exhibit a linear relationship. The second region signifies plastic deformation (10–30%), where the material undergoes permanent deformation. The third region is densification (30–50%), whereby the material undergoes a reduction in voids, leading to the formation of a more compact structure.[25,45]

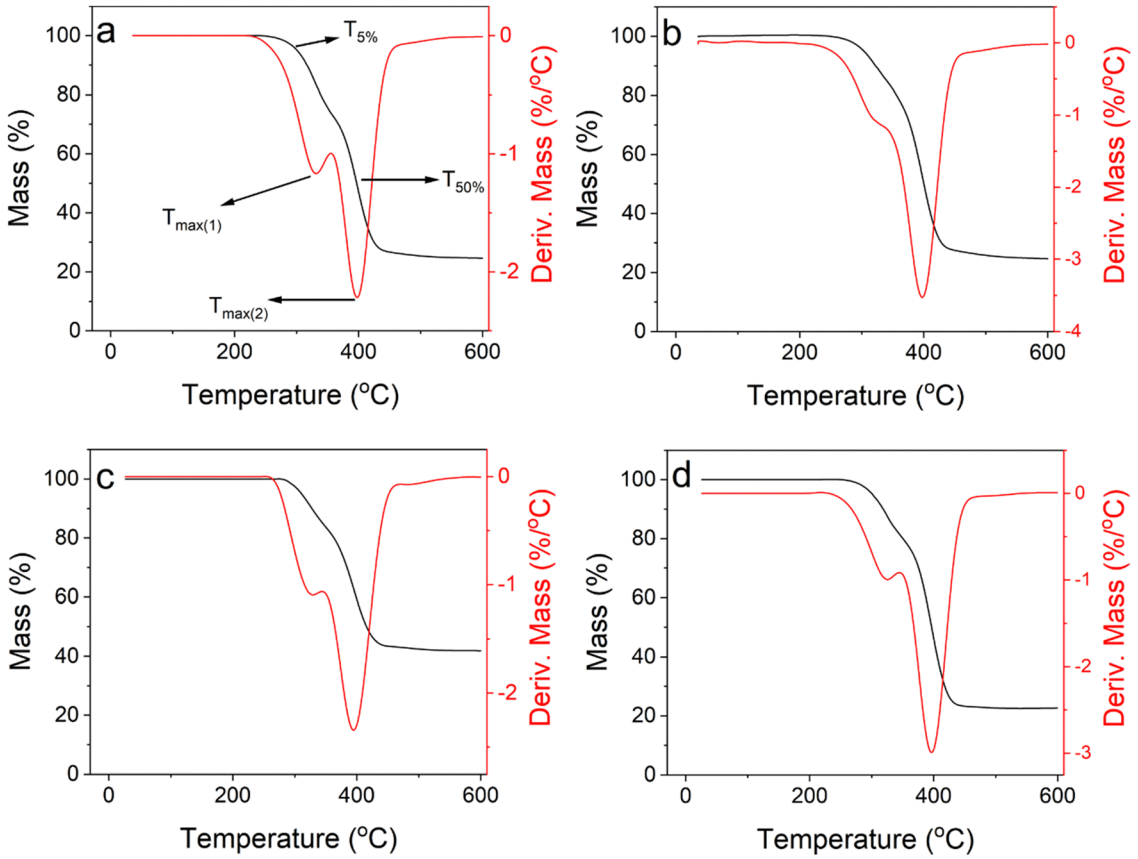

Fig. 4 TGA/DTG thermograms of (a) FPU1.05, (b) FPU1.10, (c) FPU1.15, (d) FPU1.20.

Table 4 Thermal properties of the prepared FPU samples

Sample	$T_{5\%}$ (°C)	$T_{50\%}$ (°C)	T_{max1} (°C)	T_{max2} (°C)
FPU1.05	301.36	396.89	324.04	396.18
FPU1.10	303.29	400.14	324.41	396.63
FPU1.15	310.93	415.73	329.28	396.10
FPU1.20	300.77	396.55	326.81	396.58

The results suggest that there is a direct relationship between the decrease in isocyanate index and water content, and the increase in compression strength of the foam. This can be explained by a reduction in the blowing reaction between the isocyanate and water, resulting in the reduced production of CO_2 gas. Consequently, the foam displays fewer open-cell structures and higher density, which improves its compression strength. Furthermore, FPU foams' compression properties can be closely linked to its pore morphology. Specifically, as the isocyanate index and water content decrease, the foams generate smaller cavities that may effectively resist the compression forces.

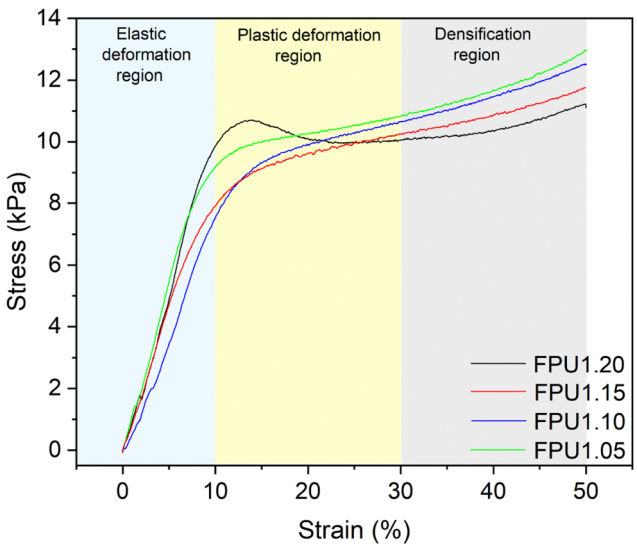

Fig. 5 Compression stress–strain behavior for FPU1.05, FPU1.10, FPU1.15 and FPU1.20.

3.7 The output voltage of FPU-based TENG

Fig. 6a–e illustrates the working principle of the FPU-based TENG one-cycle process. TENG's operation mechanism generally is based on the coupling effect, triboelectrification, and electrostatic induction.[46] In the initial position (Fig. 6a), the surfaces have no charge because the PTFE and foam are not in contact. When the two surfaces come into contact, the different electron affinities of the FPU and the PTFE film result in

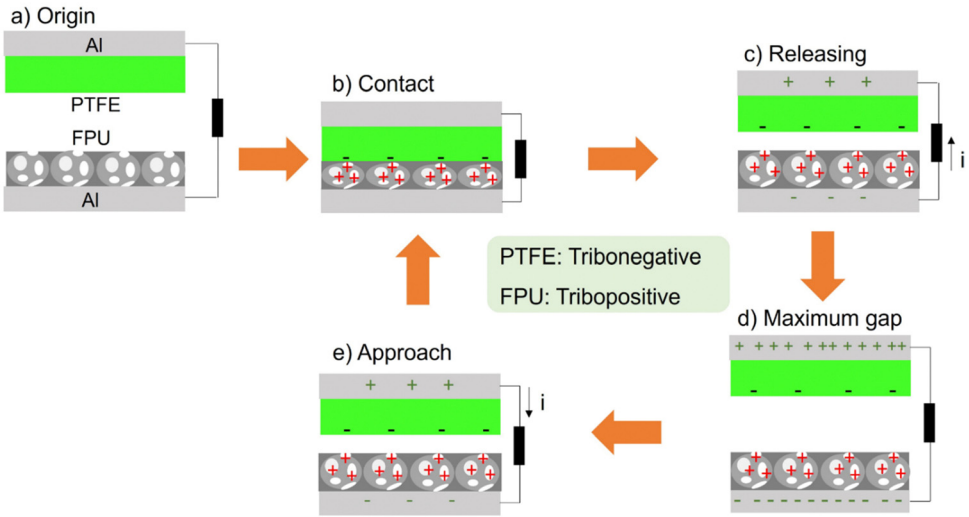

Fig. 6 (a)–(e) Schematic illustration of the operating principal of the FPU-based TENG in vertical contact-separation mode.

contact electrification at the interface, causing equivalent negative and positive charges (Fig. 6b). When PTFE begins to separate (Fig. 6c), the triboelectric charges become unbalanced. In order to attain electrical equilibrium, the positive charge on the surface of the FPU induces a negative charge on the Al electrode, causing electrons to travel from the ground to the electrode. Complete separation of the foam and PTFE surfaces (Fig. 6d) results in the induced negative triboelectric charges on the Al electrode, completely compensating for the positive triboelectric charges on the foam. When the PTFE re-approaches the surface of the foam (Fig. 6e), the induced negative charges on the Al electrode decrease, allowing the free electrons to return to the ground and resulting in an inverted output signal. This represents a single electricity generation cycle. New working cycles would begin during the periodical contact separation between the two triboelectric layers.[47,48]

3.7.1 Effect of changing the FPU density. Fig. 7a illustrates how changing the density of the FPU affects the output voltage of the TENG at various applied frequencies of 2.5, 3.75, and 5 Hz. The results indicate that a higher FPU density leads to an increase in the output voltage. For instance, the output voltage obtained was 170, 234, 252, and 273 V for densities of 17, 22, 26, and 33 kg m^{-3}, respectively, at a force of 4.8 N, a frequency of 5 Hz and a thickness of 4 mm. As an illustration, the typical open-circuit voltage for a density of 22 kg m^{-3} at a force of 4.8 N and frequency of 5 Hz and a thickness of 4 mm is displayed in Fig. 7b. Furthermore, as discussed in the next section, the output voltage is observed to increase with applied frequencies for all tested densities. The observed TENG behavior can be directly related to the change in the morphology of the FPU foams of different densities. Reducing the isocyanate index and water content makes the reaction rate slower and generates a smaller amount of CO_2. This leads to the formation of small cavities and pores, as mentioned earlier in SEM analysis. The deformation of these small cavities during the periodic contact-separation process generates extra charges on their inner walls, hence increasing the output voltage of the TENG device. In addition, the presence of small pores increases the contact area with the PTFE film when subjected to an external load, thus leading to a higher output voltage. Finally, the porosity of the FPU foams increased when the isocyanate index and water content were increased, as explained in Section 3.3. This resulted in the formation of large cavities with a significant amount of air inside the foam samples. As a result, the output voltage of the TENG decreased due to the lower electrical permittivity of air, which in turn reduced the overall relative permittivity of the FPU layer.[12]

The durability and mechanical robustness of the fabricated materials employed in TENG devices are crucial for their practical applications. As an example, the durability of an FPU-based TENG with a density of 22 kg m^{-3} was evaluated by subjecting it to continuous contact-separation for 18 000 cycles at a force of 4.8 N, as depicted in Fig. 7c. The results showed that there was no significant change in the output voltage signals of the TENG after continuous contact-separation for 18 000 cycles, indicating the mechanical robustness and durability of the fabricated foam sheet. Additionally, SEM analysis was conducted before and after 18 000 cycles at a force of 4.8 N, as shown in Fig. 7d, to further investigate the mechanical robustness of the developed foam sample. The analysis clearly showed that the foam cavities did not collapse or undergo permanent deformation after the periodic contact-separation for 18 000 cycles, confirming a stable and robust foam morphology. This stability is crucial for long-term use and, consequently, a wide range of practical applications.

3.7.2 Effect of applied force and contact frequency. Fig. 8(a)–(d) show the effect of contact frequency and FPU thickness of the four different densities on the output voltage of the TENG. It is clearly observed that the output voltage of the TENG increases with the increase in the contact frequency on the FPU-triboelectric layer. For instance, the output voltage recorded values of 104, 170, and 273 V at forces of 3.8 N,

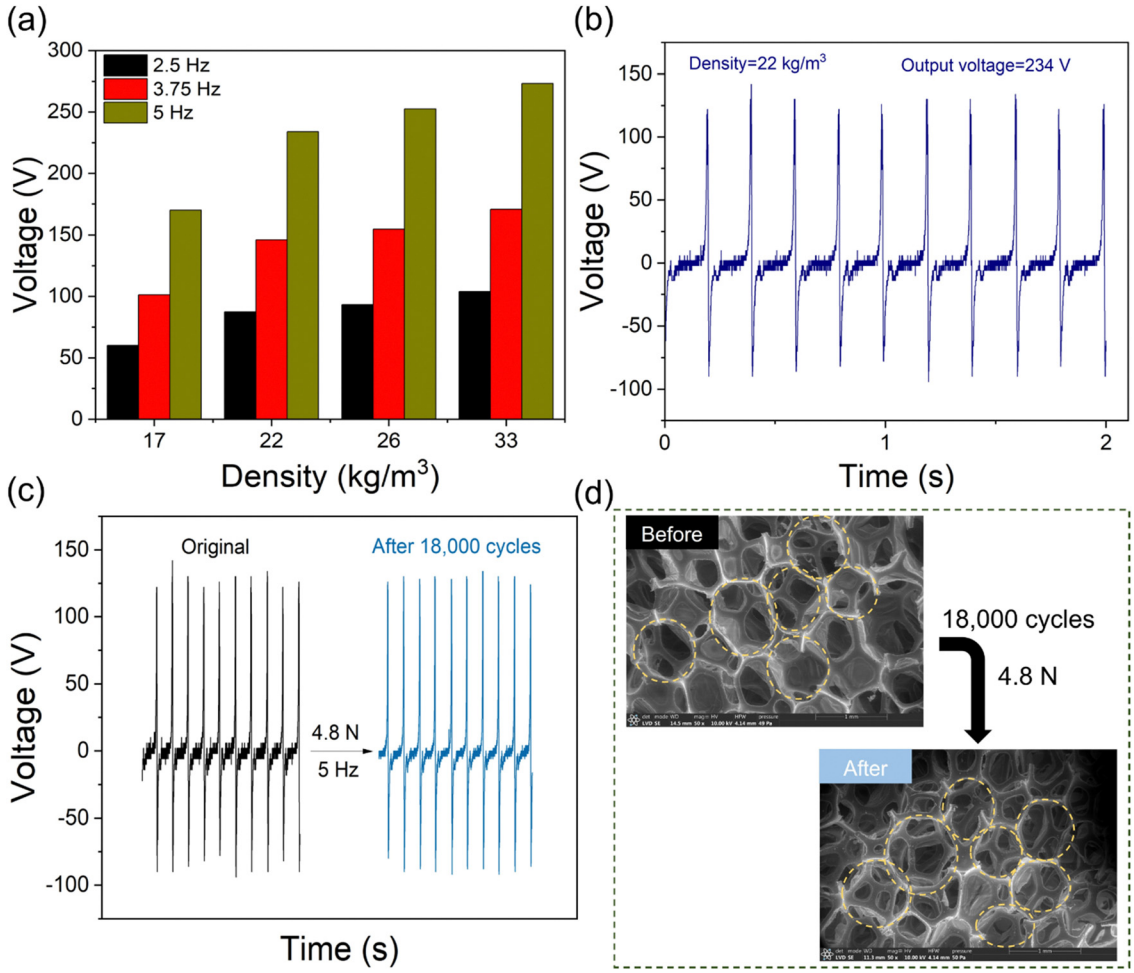

Fig. 7 (a) Density of FPU *versus* output voltage of TENG at a thickness of 4 mm; (b) output voltage of FPU foam with a density of 22 kg m^{-3} and a thickness of 4 mm under a force of 4.8 N and frequency of 5 Hz; (c) durability test of FPU1.15-based TENG over 18 000 contact-separation cycles at an applied force of 4.8 N; and (d) SEM analysis of FPU foam before and after 18 000 cycles.

4 N and 4.8 N and corresponding frequencies of 2.5, 3.75, and 5 Hz, respectively, at an FPU density of 33 kg m^{-3} and thickness of 4 mm. The increase in applied force on the FPU resulted in a larger contact area between the two materials and accelerated the rate of charge transfer at the interfaces, hence enhancing the output voltage. Moreover, increasing the contact frequency results in a decrease in the duration of contact and separation, hence diminishing the chance for charge dissipation and consequently enhancing the output voltage of TENG. Similar trends are reported in the literature.[49,50] Table 5 presents a comparison between the findings of the present study, bulk PU (without foam), and various porous materials documented in the literature. The data illustrates that the fabricated FPU foams exhibited greater output voltage in contrast to bulk PU and other porous materials. Even though the contact area of FPU samples was higher than the other materials, which can contribute to the improvement of the output voltage of the TENG device, the high elasticity, lightweight, durability and ability to vary its density make FPU an attractive choice for use in TENG for various applications.

3.7.3 Effect of increasing FPU thickness. The performance of FPU-based TENG with four different thicknesses (4, 6, 8, and 10 mm) of the FPU tribopositive layer was explored and the results are summarized in Fig. 8a–d. Four thicknesses from each density were examined at three different frequencies of 2.5, 3.75 and 5 Hz. In general, the results indicated that the output voltage of the TENG decreased as the thickness of the FPU layer increased. For example: by increasing the thicknesses from 4 to 10 mm, the output voltage dropped from 60 to 43.3 V, respectively, at a density of 17 kg m^{-3} and frequency of 2.5 Hz (Fig. 8a). A similar trend was seen across all densities and applied frequencies (Fig. 8b–d). This is believed to be due to the increase in the distance between the triboelectrification charge present on the surface of the FPU and the Al electrode, resulting in a reduction in electrostatic induction. Consequently, the output voltage of the TENG decreases.[50] Furthermore, a thicker material leads to increased stiffness, making it more resistant to deformation when a force is applied. Consequently, the induction of charges within the inner pores becomes more challenging, resulting in a decrease in the output voltage.

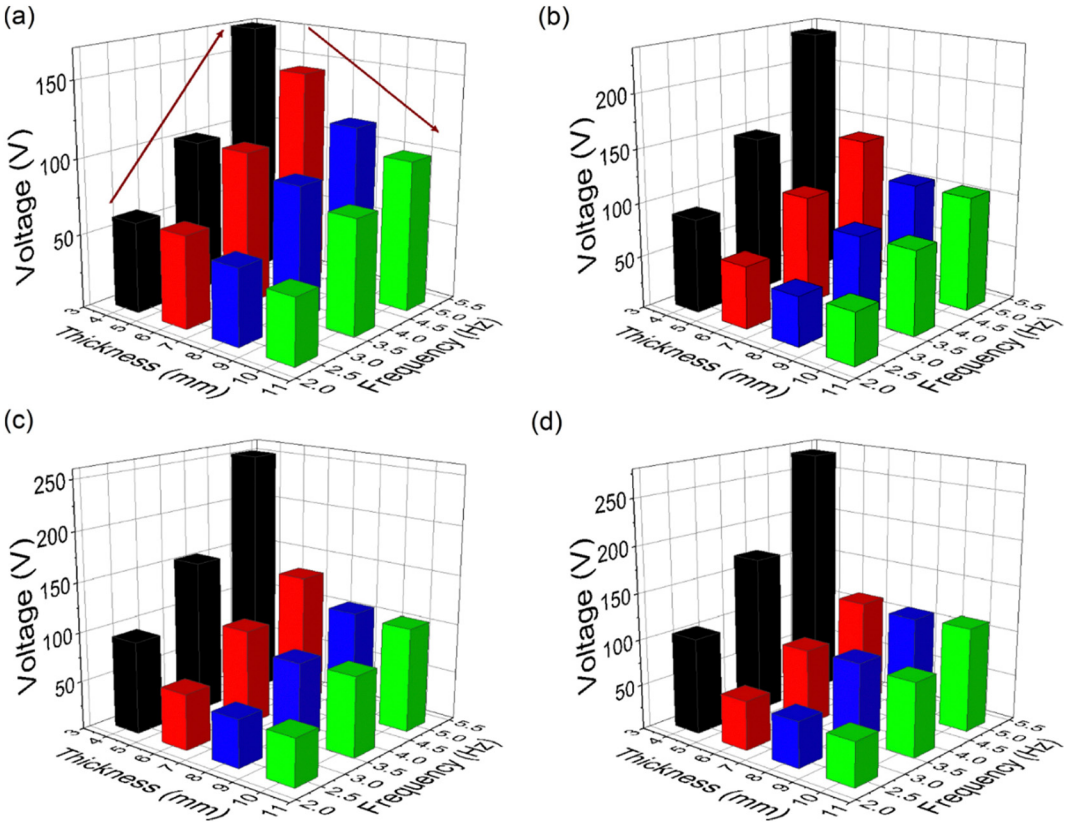

Fig. 8 The relationship between the thickness of the FPU, applied frequency and output voltage of TENG for four different densities: (a) 17, (b) 22, (c) 26, and (d) 33 kg m^{-3}.

3.8 Characterization of TENG device

To assess the performance of the developed FPU-based TENG, the TENG device that was constructed using FPU foam with a density of 33 kg m^{-3} and a thickness of 4 mm was connected to different load resistances ranging from 10–60 MΩ. The output voltage, current, and power density were then measured while maintaining a constant force of 4.8 N and a frequency of 5 Hz. Fig. 9a illustrates the changes in output current and voltage in relation to different load resistances. The findings indicated a positive correlation between the load resistance and the output voltage, with the voltage peaking at 194 V when the resistance reached 60 MΩ. In contrast, the output current reaches a maximum value of 10.2 μA when the resistance is reduced to 10 MΩ, indicating the occurrence of a short circuit. The output current was found to decrease to 3.2 μA at 60 MΩ due to ohmic losses.[12] The fabricated TENG device was used to supply power to a series connection of four commercial white Light-Emitting Diodes (LEDs) (please see ESI† Video S1). Additionally, to evaluate the effectiveness of an FPU-based TENG device, its power density, defined as the quantity of electrical power per unit area, was computed utilizing the following equations:

$$\text{Power } (P) = \frac{V^2}{R} \quad (3)$$

$$\text{Power density} = \frac{P}{A} \quad (4)$$

where V is the output voltage, R is the resistance and A is the contact area.

Table 5 Comparison of output performance of TENGs using various porous materials from literature and the findings of this study

Material	Generation mode	Applied frequency (Hz)	Force (N)	Contact area (cm^2)	Output voltage (V_{oc})	Ref.
Bulk PU	TENG	0.15	4	19.6	58.5	51
Polystyrene foam	TENG	10	90	1 × 1	130	16
PDMS sponge	TENG	1.6	6	3.7 × 3.7	181	52
Porous PTFE	TENG	30	—	2 × 2	5.1	53
Porous PVDF	TENG	10	16		90	54
FPU1.05	TENG	5	4.8	8 × 5.5	273	This work
FPU1.10	TENG	5	4.8	8 × 5.5	252	This work
FPU1.15	TENG	5	4.8	8 × 5.5	234	This work
FPU1.20	TENG	5	4.8	8 × 5.5	170	This work

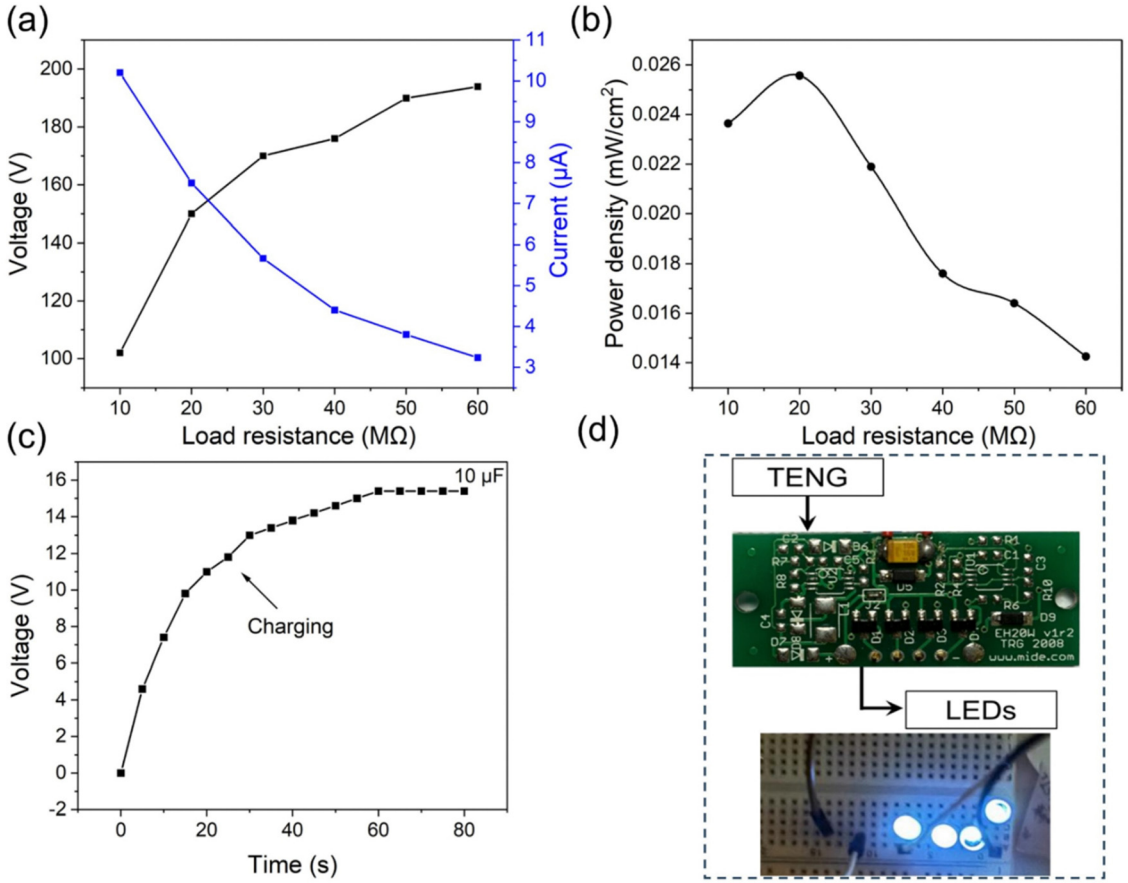

Fig. 9 Characterization of FPU-based TENG (a) variation of output voltage and output current against varying load resistances ranging from 10 to 60 MΩ, (b) power density values at different load resistances, (c) charging behavior of a 10 μF capacitor, and (d) optical image of powering four white LEDs operating at 5 Hz and 4.8 N using energy stored in a rectifier circuit.

The correlation between power density and varying load resistances is illustrated in Fig. 9b. The findings show that the developed FPU-based TENG achieved a maximum power density of 0.025 mW cm^{-2} under a resistance of 20 MΩ, a contact area of 8 × 5.5 cm^2, an applied force of 4.8 N, and a contact frequency of 5 Hz. The power density produced in this study was found to be satisfactory when compared to porous materials that have been described in the literature. For instance, Oh *et al.*[55] fabricated a highly porous TENG based on TPU/PP layers for energy harvesting through human motion. The findings showed that at an applied force and frequency of 5 N and 8 Hz, respectively, the maximum power density at a load resistance of 10 MΩ was 0.9 μW cm^{-2}. In another study, Gokarna *et al.*[56] designed a TENG device for energy harvesting applications using an ultrathin porous PU membrane. The results indicated that the developed TENG obtained a maximum power density of 9.7 mW m^{-2} at a load resistance of 40 MΩ, a force of 4 N, and a contact area of 19.6 cm^2.

In order to assess the charging capabilities of the constructed FPU-based TENG, it was connected to a rectifier circuit (model: Mide EH20W) with a capacitance of 10 μF. The capacitor's charging behavior curve is presented in Fig. 9c. It is evident that the TENG device charges the 10 μF capacitor and reaches a maximum value of 15.4 V in about 60 seconds, indicating the device's capability for rapid energy storage. The formula $E = \frac{1}{2}CV^{2}$[48] can be employed to quantify the energy storage capacity, where E represents the energy stored, C denotes the capacitance of the capacitor, and V signifies the output voltage. It was found that the developed FPU-based TENG device could store 1185.8 μJ of energy using the 10 μF capacitor. Practically, this energy was effectively converted into power for four commercial white LEDs, as illustrated in Video S2 (ESI†) and Fig. 9d. Thus, the fabricated FPU-based TENG has a great potential for energy harvesting in microelectronic devices.

4. Conclusions

In this work, we conducted a thorough investigation to examine how modifying the density and thickness of the FPU triboelectric layer impacts the output voltage of the TENG device. Through the adjustment of the isocyanate index and water content during the foam preparation process, we were able to successfully produce four different densities of FPU foam. The chemical structure and morphology of FPU foams was

investigated using the FTIR and FESEM techniques, respectively. The results demonstrated that higher isocyanate index and water content lead to an increased production of CO_2 gas, resulting in the formation of larger cavities and pore diameters. As a consequence, the density of the FPU decreased while its porosity increased. In addition, the prepared foams' thermal stability was explored using a TGA device. The results showed that increasing the isocyanate index (1.05–1.15) and water content provides the foam structure with some rigidity, which arises from the pi-stacking of aromatic rings of the isocyanate, thus increasing thermal stability. The compression performance of the obtained foams was also examined, and the findings showed that the compression strength increased with a decrease in isocyanate index and water content. In addition, we examined how the applied force and contact frequency, FPU density, and FPU thickness impact the output voltage of the TENG device. The results demonstrated that higher applied frequencies and greater FPU densities positively influenced the output voltage. On the other hand, increasing the thickness of the FPU layer had an adverse effect, reducing the TENG's output voltage. In addition, the maximum power density of the FPU-based TENG device at a resistance of 20 MΩ, force of 4.8 N, and frequency of 5 Hz was found to be 0.025 mW cm^{-2} for an FPU thickness of 4 mm and density of 33 kg m^{-3}. In addition, this device was capable of rapidly charging a 10 μF capacitor to 15.4 V in 60 seconds, with an estimated energy storage of 1185.8 μJ. The findings of our study lead to the conclusion that by adjusting the density and thickness of FPU foam, we may effectively optimize the performance of TENG. Moreover, this work introduces a simple, cost-effective and sustainable energy harvesting device that can be utilized to supply power to electronic devices.

Conflicts of interest

There are no conflicts to declare.

Acknowledgements

This research was supported by the American University in Cairo under the internal grant agreement number SSE-MENG-A.E-FY22-RG-2022-Nov-10-19-38-38.

References

1 I. Dincer, *Renewable Sustainable Energy Rev.*, 2000, **4**, 157–175.
2 A. Midilli, M. Ay, I. Dincer and M. A. Rosen, *Renewable Sustainable Energy Rev.*, 2005, **9**, 255–271.
3 F.-R. Fan, Z.-Q. Tian and Z. L. Wang, *Nano Energy*, 2012, **1**, 328–334.
4 X. Cao, Y. Jie, N. Wang and Z. L. Wang, *Adv. Energy Mater.*, 2016, **6**, 1600665.
5 J. Chen and Z. L. Wang, *Joule*, 2017, **1**, 480–521.
6 G. Zhu, C. Pan, W. Guo, C.-Y. Chen, Y. Zhou, R. Yu and Z. L. Wang, *Nano Lett.*, 2012, **12**, 4960–4965.
7 S. Wang, L. Lin and Z. L. Wang, *Nano Lett.*, 2012, **12**, 6339–6346.
8 R. Dharmasena and S. Silva, *Nano Energy*, 2019, **62**, 530–549.
9 A. Ahmed, I. Hassan, A. M. Pourrahimi, A. S. Helal, M. F. El-Kady, H. Khassaf and R. B. Kaner, *Adv. Mater. Technol.*, 2020, **5**, 2000520.
10 F. R. Fan, W. Tang and Z. L. Wang, *Adv. Mater.*, 2016, **28**, 4283–4305.
11 Y. S. Choi, S. W. Kim and S. Kar-Narayan, *Adv. Energy Mater.*, 2021, **11**, 2003802.
12 Z. Saadatnia, S. G. Mosanenzadeh, T. Li, E. Esmailzadeh and H. E. Naguib, *Nano Energy*, 2019, **65**, 104019.
13 H.-Y. Mi, X. Jing, Q. Zheng, L. Fang, H.-X. Huang, L.-S. Turng and S. Gong, *Nano Energy*, 2018, **48**, 327–336.
14 Q. Zheng, L. Fang, H. Guo, K. Yang, Z. Cai, M. A. B. Meador and S. Gong, *Adv. Funct. Mater.*, 2018, **28**, 1706365.
15 M. M. Rastegardoost, O. A. Tafreshi, Z. Saadatnia, S. Ghaffari-Mosanenzadeh, C. B. Park and H. E. Naguib, *Nano Energy*, 2023, **111**, 108365.
16 K. Y. Lee, J. Chun, J.-H. Lee, K. N. Kim, N.-R. Kang, J.-Y. Kim, M. H. Kim, K.-S. Shin, M. K. Gupta and J. M. Baik, *Adv. Mater.*, 2014, **26**, 5037–5042.
17 D. Kamaruzaman, N. S. M. Mustakim, A. S. R. A. Subki, N. Parimon, M. K. Yaakob, M. F. Malek, N. Vasimalai, M. H. Abdullah, S. A. Bakar and M. K. Ahmad, *Mater. Today Sustainability*, 2024, **26**, 100726.
18 L. Ren, *Mater. Technol.*, 2022, **37**, 1140–1145.
19 M. Wu, Z. Gao, K. Yao, S. Hou, Y. Liu, D. Li, J. He, X. Huang, E. Song and J. Yu, *Mater. Today Energy*, 2021, **20**, 100657.
20 T. G. Weldemhret, D.-W. Lee, Y. T. Park and J. I. Song, *Chem. Eng. J.*, 2022, **450**, 137982.
21 M. Zhi, Q. Liu, Y. Zhao, S. Gao, Z. Zhang and Y. He, *ACS Omega*, 2020, **5**, 2734–2746.
22 A. Maamoun, A. El-Wakil and T. M. El-Basheer, *J. Cell. Plast.*, 2022, **58**(4), 645–672.
23 P. Scarfato, L. Di Maio and L. Incarnato, *Composites, Part B*, 2017, **109**, 45–52.
24 R. Deng, P. Davies and A. Bajaj, *J. Sound Vib.*, 2003, **262**, 391–417.
25 A. Maamoun and A. Mahmoud, *Cellulose*, 2022, **29**, 6323–6338.
26 S. Dworakowska, D. Bogdał, F. Zaccheria and N. Ravasio, *Catal. Today*, 2014, **223**, 148–156.
27 M. Ionescu, *Chemistry and technology of polyols for polyurethanes*, iSmithers Rapra Publishing, 2005.
28 S. A. Baghban, M. Khorasani and G. M. M. Sadeghi, *J. Appl. Polym. Sci.*, 2019, **136**, 47363.
29 A. A. Maamoun, D. M. Naeim, A. A. Mahmoud, A. M. Esawi and M. Arafa, *Nano Energy*, 2024, **124**, 109426.
30 Y. Liu, Y. Zheng, Z. Wu, L. Zhang, W. Sun, T. Li, D. Wang and F. Zhou, *Nano Energy*, 2021, **79**, 105422.
31 H. Choe, G. Sung and J. H. Kim, *Compos. Sci. Technol.*, 2018, **156**, 19–27.
32 M. Kardeş, H. C. Yatmaz and K. Öztürk, *ACS Appl. Nano Mater.*, 2023, **6**, 6605–6613.

33 F. Zhou, T. Zhang, B. Zou, W. Hu, B. Wang, J. Zhan, C. Ma and Y. Hu, *Polym. Degrad. Stab.*, 2020, **171**, 109029.
34 K. Cole, P. Van Gheluwe, M. Hébrard and J. Leroux, *J. Appl. Polym. Sci.*, 1987, **34**, 395–407.
35 L. Zhang, H. K. Jeon, J. Malsam, R. Herrington and C. W. Macosko, *Polymer*, 2007, **48**, 6656–6667.
36 R. Hodlur and M. Rabinal, *Compos. Sci. Technol.*, 2014, **90**, 160–165.
37 S. H. Baek and J. H. Kim, *Compos. Sci. Technol.*, 2020, **198**, 108325.
38 G. Sung and J. H. Kim, *Compos. Sci. Technol.*, 2017, **146**, 147–154.
39 S.-T. Lee and N. S. Ramesh, *Polymeric foams: mechanisms and materials*, CRC Press, 2004.
40 M. Karimi, S. Seddighi and R. Mohammadpour, *Sci. Rep.*, 2021, **11**, 16191.
41 Z. Saadatnia, S. G. Mosanenzadeh, E. Esmailzadeh and H. E. Naguib, *Sci. Rep.*, 2019, **9**, 1370.
42 A. Lapprand, F. Boisson, F. Delolme, F. Méchin and J.-P. Pascault, *Polym. Degrad. Stab.*, 2005, **90**, 363–373.
43 A. A. Septevani, D. A. Evans, C. Chaleat, D. J. Martin and P. K. Annamalai, *Ind. Crops Prod.*, 2015, **66**, 16–26.
44 X. Liu, J. Hao and S. Gaan, *RSC Adv.*, 2016, **6**, 74742–74756.
45 T.-T. Li, W. Dai, S.-Y. Huang, H. Wang, Q. Lin, C.-W. Lou and J.-H. Lin, *Mater. Des.*, 2019, **183**, 108150.
46 R. Ccorahua, J. Huaroto, C. Luyo, M. Quintana and E. A. Vela, *Nano Energy*, 2019, **59**, 610–618.
47 T. G. Weldemhret, D.-W. Lee, M. Prabhakar, Y. T. Park and J. I. Song, *ACS Appl. Nano Mater.*, 2022, **5**, 12464–12476.
48 G. M. Rani, C.-M. Wu, K. G. Motora and R. Umapathi, *J. Cleaner Prod.*, 2022, **363**, 132532.
49 S. Wang, L. Ding, Y. Wang and X. Gong, *Nano Energy*, 2019, **59**, 434–442.
50 L. Shi, S. Dong, H. Xu, S. Huang, Q. Ye, S. Liu, T. Wu, J. Chen, S. Zhang and S. Li, *Nano Energy*, 2019, **64**, 103960.
51 D. S. Mahmoud, S. H. El-Sabbagh, T. M. El-Basheer, A. Moustafa and M. A. Barakat, *J. Thermoplast. Compos. Mater.*, 2023, **36**, 4684–4706.
52 Z. Peng, J. Song, Y. Gao, J. Liu, C. Lee, G. Chen, Z. Wang, J. Chen and M. K. Leung, *Nano Energy*, 2021, **85**, 106021.
53 M. Wang, N. Zhang, Y. Tang, H. Zhang, C. Ning, L. Tian, W. Li, J. Zhang, Y. Mao and E. Liang, *J. Mater. Chem. A*, 2017, **5**, 12252–12257.
54 M. Wang, W. Liu, X. Shi, J. Pan, B. Zhou, J. Wang, T. Sun and Y. Tang, *New J. Chem.*, 2021, **45**, 1893–1898.
55 H. J. Oh, J. H. Bae, Y. K. Park, J. Song, D. K. Kim, W. Lee, M. Kim, K. J. Heo, Y. Kim and S. H. Kim, *Polymers*, 2020, **12**, 1044.
56 M. Gokana, C.-M. Wu, U. Reddicherla and K. Motora, *eXPRESS Polym. Lett.*, 2021, **15**, 1019–1031.